Reversible Chirality Control in Peptide-Functionalized Gold Nanoparticles

Edoardo Longo, Andrea Orlandin, Fabrizio Mancin, Paolo Scrimin,* and Alessandro Moretto*

Department of Chemical Sciences, University of Padova, Via Marzolo 1, 35131 Padova, Italy

ABSTRACT We report the induction of chiroptical properties in 2 nm diameter gold nanoparticles passivated with short peptides characterized by the Aib-L-Ala repetition in their sequence. The nanoparticles present relevant ECD signals in the 300−650 nm wavelength region, corresponding to the gold nanoparticle's quantized electronic structure. Although the only chiral amino acid present in the peptide sequences is L-Ala, the particles show mirror image spectra like those of enantiomers according to the number of amino acids in the main chain (odd or even). Such a behavior appears to be strongly influenced by the secondary structure assumed by the peptides when passivating the nanoparticles and vanishes when the sequence is long enough to assume a 3_{10}-helix conformation. Moreover, chirality control is a reversible process and can be deactivated or reactivated by increasing or decreasing the temperature.

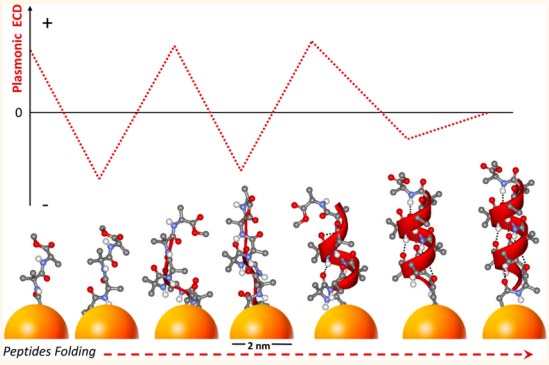

KEYWORDS: chiral gold nanoparticle · peptide gold nanoparticle · helical peptide · circular dichroism · supramolecular chemistry

Chirality of gold nanoparticles is an intriguing property that only recently has started to become the focus of investigation. The role of the passivating monolayer in affecting it has not been fully understood yet. Peptide-functionalized gold nanoparticles[1−3] constitute appealing supramolecular systems for their ability to mimic natural proteins. By confining on the surface of a cluster of gold atoms several copies of a peptide, a nanosystem that resembles a protein in size (a few nanometers), shape (globular), and, possibly, function may be obtained.[4] Peptide-functionalized gold nanoparticles have been used, *inter alia*, in catalysis,[5−8] selective protein recognition,[9,10] drug delivery,[11,12] and gene transfection.[13,14] However, in spite of the chiral properties deriving from the helical conformation and the configuration of the constituent amino acids, chirality in peptide-functionalized gold nanoparticles has been little explored. After the first observation by Whetten[15] of optical activity of glutathione (a tripeptide)-passivated gold nanoparticles, the few other examples are constituted by peptide nanotubes,[16] cysteine,[17,18] and unstructured peptides.[19] It is now well accepted that chirality in such nanosystems may derive from[19,20] (a) the chiral arrangement of the metal cluster of the gold core; (b) the binding of the thiolates on the gold surface to form chirally arranged staples (a bridged binding motif involving gold and sulfur);[21] and (c) the chirality of the surrounding monolayer of passivating organic molecules. Peptide sequences rich in C^{α}-tetrasubstituted α-amino acids are known to stabilize the metallic cluster of gold nanoparticles in very polar solvents.[22,23] This is likely associated with their strong propensity to fold into rather robust 3_{10}- or α-helix conformations. We argued that these properties could be exploited to address: (a) peptide folding behavior when bound to the surface of a gold nanoparticle; (b) the role of the individual amino acids and the secondary structure of the sequence in inducing chiroptical properties to the passivated nanoparticles.

RESULTS AND DISCUSSION

In this view, we synthesized by conventional solution protocols seven peptides with Aib (α-amino isobutyric acid) and L-Ala alternating residues and *N*-mercaptopropionyl (m*pr*-) N-termination (**P2**−**8**; see Figure 1).

Even sequences are characterized, at the N-terminus, by an Aib amino acid, while odd

* Address correspondence to paolo.scrimin@unipd.it, alessandro.moretto.1@unipd.it.

Received for review July 23, 2013 and accepted October 15, 2013.

Published online October 16, 2013
10.1021/nn403816a

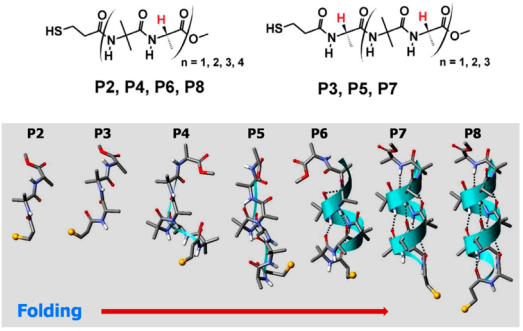

Figure 1. (Top) Chemical structure of peptides used for the passivation of the gold nanoparticles: P2, m*pr*-Aib-Ala-OMe; P3, m*pr*-Ala-Aib-Ala-OMe; P4, m*pr*-(Aib-Ala)$_2$-OMe; P5, m*pr*-Ala-(Aib-Ala)$_2$-OMe; P6, m*pr*-(Aib-Ala)$_3$-OMe; P7, m*pr*-Ala-(Aib-Ala)$_3$-OMe; P8, m*pr*-(Aib-Ala)$_4$-OMe. (Bottom) Conformation of the peptides as inferred from their ECD and FT-IR spectra in solution (see Supporting Information (SI)).

ones by a L-Ala amino acid because our optimized synthetic protocol uses L-Ala as the C-terminus starting amino acid. As some of us already reported for similar oligopeptides, **P2**−**8** progressively fold in water according to the peptide length (see Figure 1, bottom).[24] The critical main-chain length for the transition from a random coil to a helix structure in this solvent, as inferred from the electronic circular dichroism (ECD) and Fourier transform infrared (FT-IR) spectra (see Figure S1 of the SI), is six residues. These oligopeptides were then used to passivate gold nanoparticles AuNp**2**−**8**. The nanoparticles were prepared by one-phase $NaBH_4$ reduction of $HAuCl_4$ in water/methanol and in the presence of a 2-fold molar excess of the peptides. Transmission electron microscopy (TEM) and thermogravimetric analysis (TGA) (see Figures S2−4 of the SI) provide the relevant characterization data summarized in Table 1. While the diameters of the obtained AuNp**2**−**8** are fairly constant in the 2.0−2.4 nm range (Figure S3 of the SI), there is a huge decrease in the number of peptides necessary to fully passivate the gold cluster surface as the sequence elongates.

In the series the number of peptides decreases from 126 for AuNp**2** to 27 for AuNp**8**. This implies a larger surface coverage exerted by longer peptides (footprint increases from *ca.* 0.1 nm^2 for AuNp**2** and AuNp**3** to 0.2 nm^2 for AuNp**5** and eventually to *ca.* 0.7 nm^2 for AuNp**8**). The footprint values, *i.e.*, the size of the area occupied by the projection of a peptide on the gold surface, obtained for AuNp**2**,**3** are similar to those reported for gold nanoparticles passivated by alkylthiols[25] or short poly(Aib)[26] sequences and indicate a dense packing of the coating. Such a trend correlates well with the different conformations assumed by the peptides on the particles as revealed by the ECD spectra (Figure 2A). The behavior is partially different with respect to that observed for the peptides in solution (see the SI). AuNp**2** and AuNp**4** display a negative dichroism at 200 nm with concomitant weak positive dichroism at 215−220 nm, suggesting an unordered conformation. On the other hand, AuNp**3** presents a negative band at *ca.* 235 nm, suggesting a β-sheet-like contribution. Such a conformation is still present in AuNp**5** although the negative band that starts to develop at *ca.* 205 nm may hint at some helical contribution to the overall conformation.

TABLE 1. Chemical Structure Data for All Peptide-Capped AuNp2−8 Reported in This Work

entry	core *d* (nm)[a]	Au atoms for AuNp[b]	pep. chains for AuNp[c]	footprint[d] (nm^2)
AuNp**2**	2.0 ± 0.2	247	126	0.10
AuNp**3**	2.2 ± 0.1	329	138	0.11
AuNp**4**	2.3 ± 0.2	376	119	0.14
AuNp**5**	2.0 ± 0.1	247	55	0.23
AuNp**6**	2.3 ± 0.2	376	54	0.31
AuNp**7**	2.4 ± 0.2	427	33	0.45
AuNp**8**	2.4 ± 0.2	427	27	0.68

[a] *d* = diameter. Calculated by averaging the size of at least 200 nanoparticles. [b] Calculated assuming a spherical model (see SI). [c] Determined combining TEM and TGA analysis as described in the SI. [d] Footprint: the area occupied by the projection of the peptide ligand on the gold cluster surface.

As it happens in solution, the formation of a significant amount of helix (negative bands at 208 and 220 nm) requires at least a hexameric sequence. However, when compared to the spectra of the free, unbound peptides (Figure S1 of the SI), those of the AuNps indicate that the helical content is lower for identical sequences when bound to the nanocluster surface. This structural information suggests also a plausible explanation for the observation we have made above concerning the number of peptides required for the passivation of the gold cluster. Peptides **P2**−**4** are likely in an extended conformation (little ordered or β-sheet-like) that allows a dense packing on the nanoparticle surface. On the contrary, peptides **P6**−**8** start developing a helical conformation (that of a 3_{10}-helix for **P8**) and become consequently bulkier. A simple calculation reveals that a 3_{10}-helix displays a (circular) axial backbone footprint close to 0.55 nm^2 [considering a distance (side chain)$_i$ → (side chain)$_{i+1}$, of *ca.* 8.3 Å], while that of an extended conformation (elliptical) is close to 0.12 nm^2 (considering two sections, C═O$_i$ → C═O$_{i+1}$, of *ca.* 3.8 Å and a distance (side chain)$_i$ → (side chain)$_{i+1}$, of *ca.* 4.3 Å). These figures are fully consistent with the data of Table 1 and provide a rationale for their interpretation.

Figure 2B reports the FTIR absorption spectra in the C═O stretching region for AuNp**2**−**8** in *deuterated* water. The spectra look very similar to those of free peptides **P2**−**8** (Figure S6 of the SI) but for the relevant presence of a strong absorption band at 1558 cm^{-1} in the spectrum of AuNp**2**. This band is typical of the amide II band when the spectra are recorded in H_2O and not in D_2O. Noteworthy, it slowly disappears when the solution is heated at 50 °C, while that at 1440 cm^{-1} increases (Figure S5 of the SI). This suggests that, contrary to all the other peptides bound to the

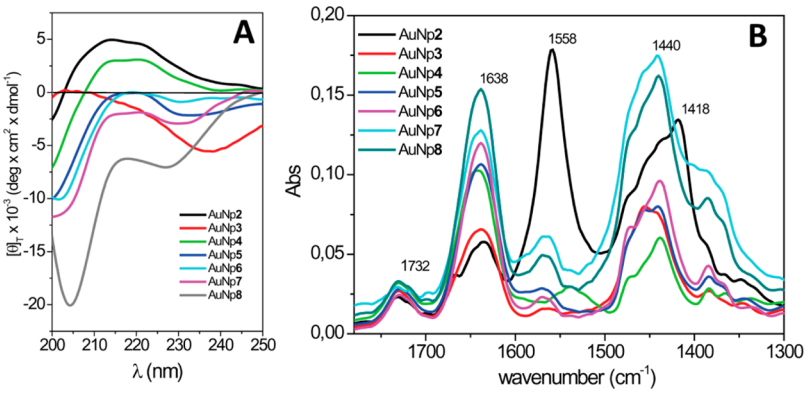

Figure 2. (A) Far-UV ECD spectra of AuNp2−8 recorded in water at 20 °C. Concentration: 1 mM. (B) FT-IR absorption spectra of AuNp2−8 recorded in D_2O at 20 °C.

nanoparticle surface, AuNp**2** presents a NH group that is involved in a relatively strong H-bond and exchanges with D_2O only very slowly. This aspect will be further discussed below. In general, all nanoparticles present very broad amide I bands, likely corresponding to the overlap of those arising from different secondary structures. In fact, second-order derivative deconvolution (Figure 3) of the signals evidences again a relevant difference between odd and even peptide-coated nanoparticles. The latter (AuNp**2**, AuNp**4**, and AuNp**6**) show only two bands at 1630 and 1645 cm^{-1}, respectively, which could arise from random and turn structures;[27,28] on the other hand, nanoparticles coated with odd peptides AuNp**3**, AuNp**5**, and AuNp**7** display also a shoulder, albeit weak, at 1665 cm^{-1} not observed in the related free peptides (Figure S6 of the SI). Such a band has been attributed to the formation of a parallel β-sheet conformation for an amyloid-derived peptide bound to a gold nanoparticle.[29]

The most remarkable properties of AuNp**2**−**8** are the chiroptical ones. In fact, AuNp**2**−**8** present a dichroic spectrum also in the 300−650 nm region (Figure 4A), which can be attributed to the gold core, with quite an interesting pattern. First of all, the intensity of the bands is larger for shorter sequences than for longer ones, and the spectrum of AuNp**8**, *i.e.*, the most helical peptide, is practically flat. Second, the spectra show almost inverted ellipticities as a function of the amino acid closest to the gold surface and, consequently, the number of amino acids in the sequence as shown in Figure 4B. The best comparison can be done for AuNp**2** and AuNp**3**, characterized by the strongest signals. The ECD spectrum of AuNp**2** presents two positive bands located at 505 and 560 nm and, in the 300−450 nm region, a set of alternating, intense bands. The spectrum of AuNp**3** shows, on the contrary, a large negative band located at 550 nm in addition to a positive band at 440 nm and a strong negative one at 340 nm. Thus the odd and even peptide sequences show mirror image spectra like those of enantiomers as far as their ECD is concerned. This alternating pattern continues along the series, although the intensity of the bands progressively decreases as the ordered structure of the sequences increases (Figure 4B, red squares and green triangles). It must be noted that passivation of the surface with even and odd peptides implies the presence, respectively, of an achiral amino acid (Aib: AuNp**2**, AuNp**4**, AuNp**6**) or a chiral one (L-Ala: AuNp**3**, AuNp**5**, AuNp**7**) close to the gold surface.

Bürgi and co-workers demonstrated that $Au_{38}(SCH_2CH_2Ph)_{24}$ is a chiral nanoparticle and successfully achieved the separation of the enantiomers and measured their CD spectra.[30] The presence of a chiroptical signal in spite of the fact that the protecting thiolate is achiral demonstrates the intrinsic chirality of the cluster. The X-ray structure of this nanoparticle reveals the presence of a staple-type binding motif between gold and sulfur, in which a gold atom is stabilized between two thiolate ligands.[31] The staples occur in two fashions, dimeric ($Au_2(SR)_3$) and monomeric ($Au(SR)_2$). The chirality of the nanoparticle derives from the propeller-like arrangement of the staples. The patterns shown in Figure 4A are quite similar to those recently reported by Bürgi and co-workers[32] for another chiral gold cluster, namely, $Au_{40}(SCH_2CH_2Ph)_{24}$, where chiroptical properties are supposed to arise from the formation of chirally arranged staples on the gold surface. This similarity is striking and could suggest that, depending on the Aib-L-Ala order in the peptide sequence (or, more likely, the amino acid that is closest to the Au surface), one of the two possible enantiomeric staples is preferentially formed also in our nanoparticles. If this were the case, for each peptide, we are not dealing with enantiomeric nanoparticles but with diastereomeric ones, since the chirality of the peptide is maintained while that due to the staple is inverted. However, the almost mirror image of the ECD spectra indicates that most of the chiroptical signal derives from the chirality on the gold surface (chiral staples) and not from the chirality of the amino acids or from the helical conformation of the peptides. In facts, the full formation of a helical conformation kills ellipticity in AuNp**8**, as shown in Figure 4A and B. This means that helix

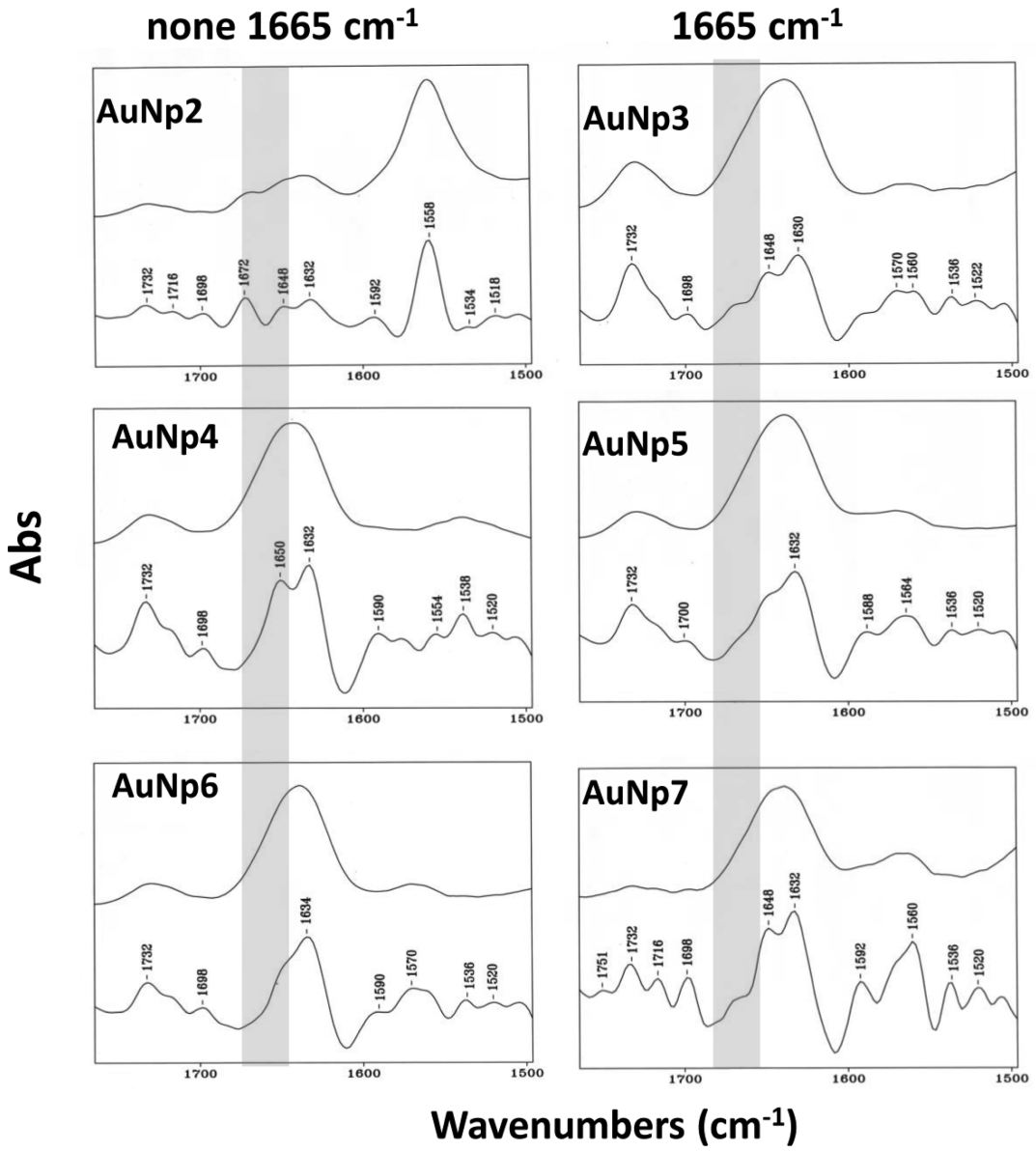

Figure 3. Second-order derivative deconvolution (bottom trace) of FT-IR absorption spectra (top trace) of AuNp2−7 recorded in D_2O at 20 °C. The dotted line represents the wavelength at which the band attributed to β-sheet formation should be present.

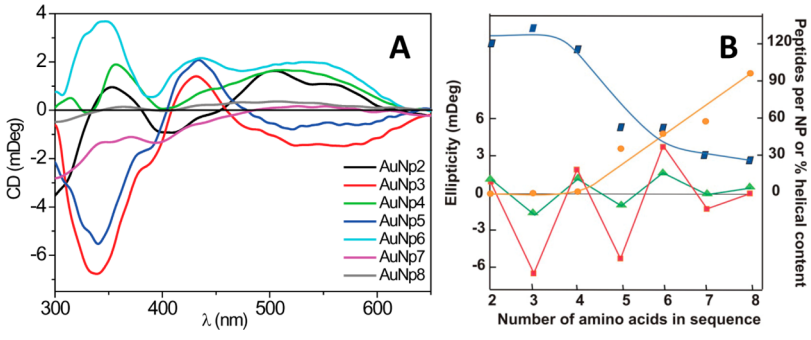

Figure 4. (A) ECD spectra of AuNps2−8 in H_2O at 20 °C in the 300−650 nm region. (B) Dependence of the percentage of helical content relative to AuNp8 (orange circles), the number of peptides per nanoparticle (blue diamonds), and the ellipticity at 340 nm (red squares) and 500 nm (green triangles) on the number of amino acids in the sequence of the peptides passivating nanoparticles AuNp2−8. Solid lines were drawn to guide the eye.

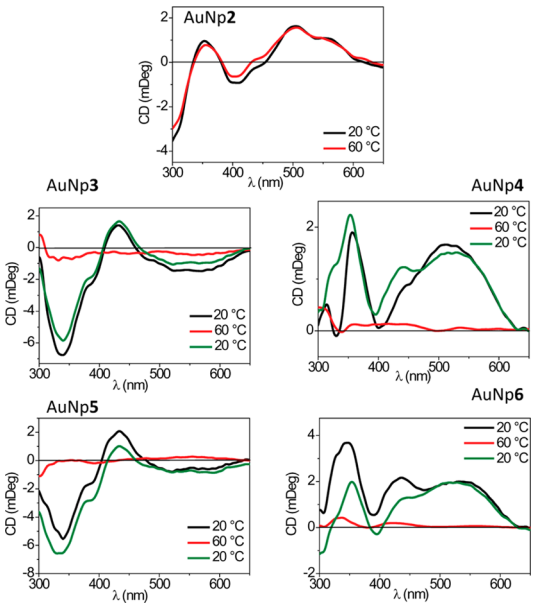

Figure 5. ECD spectra of AuNps2−6 recorded at different temperatures in H_2O. The black and green traces were recorded at 20 °C: black before heating and green after heating at 60 °C for 1 h and cooling back to 20 °C; red traces were recorded after 1 h at 60 °C.

formation either does not allow the formation of staples, for steric reasons, or prevents a critical intermolecular interaction for the selection of the stereogenic units. The stereogenic selection could be in this case associated with the possible locking of the chiral staples in one of the two chiral conformations *via* interpeptide H-bond formation (similar to a β-sheet) or a N−H hydrogen bonding to a thiol connected to the Au atoms, thus locking the first amino acid in a precise conformation. The possibility of such interaction appears particularly evident for AuNp**2**, as suggested by the presence of the very-difficult-to-exchange N−H bond associated with the 1558 cm^{-1} band in the FT-IR spectrum of Figure 2B. Selective involvement of intermolecular H-bonds is also supported by the observation of β-sheet-like features in the ECD and FT-IR spectra only for the particles coated with peptides **P3** and **P5** and not for those coated with **P2** and **P4** (Figures 2A and 3). However, the strongest support for weak (and hence reversible) interactions controlling nanoparticle chirality is provided by the ECD spectra recorded for AuNp**2**−**6** after incubation at 60 °C for one hour (Figure 5).

With the exception of AuNp**2**, the dichroic signals practically disappear, but they reappear almost with the same shape and intensity upon cooling back to 20 °C. This implies that the disappearance of the ECD signal is due to the loss of the intramolecular interactions that favor a chiral staple structure over the other, with consequent racemization of the staples in a process similar to that recently reported by Bürgi.[33] The reappearance of the ECD signals at low temperature indicates that the chiral selection corresponds to an

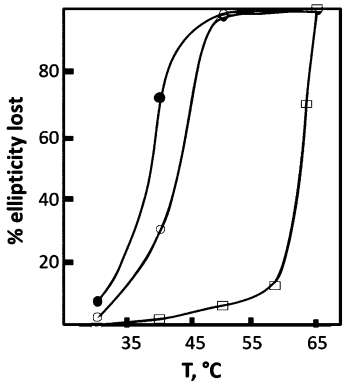

Figure 6. Percentage of ellipticity lost by AuNp2, squares, AuNp3, empty circles, and AuNp4, filled circles, when equilibrated at different temperatures. From the above points one may estimate, for the series, the following T_m values: 62, 43, 38 °C. Solid lines were drawn to guide the eye. The wavelengths at which the ellipticity values have been determined are 510 nm for AuNp2, 340 nm for AuNp3, and 510 nm for AuNp4. Equilibration kinetics are reported in Figure S8 of the SI.

energetic minimum related to the formation of two diastereomeric nanosystems. The failure of AuNp**2** to significantly lose its ECD signal after 1 h at 60 °C is in full agreement with the presence of a very strong H-bond involving one NH when peptide **P2** covers the gold surface as discussed above. Indeed, a higher temperature is required in this case for the full loss of the ellipticity (see Figure 6). Because of the reversibility of the process, by recording the ECD spectra at different temperatures, one would expect, upon equilibration, a partial loss of the ellipticity, corresponding to a new reached equilibrium in which part of the nanoparticles are no longer locked in the chiral conformation. This has been proven by using the most stable nanosystems: AuNp**2**−**4**. The plots of the percentage of ellipticity loss *versus* the temperature are reported for these nanoparticles in Figure 6.

The shape of the three curves reported in Figure 6 indicates that the loss of ellipticity is a cooperative process very similar to the denaturation of a protein. The three loss-of-ellipticity midpoint temperatures, T_m, decrease from 60 °C for AuNp**2** to 43 °C for AuNp**3** and 38 °C for AuNp**4**, indicating a loss of stability of the chirality-inducing interaction as the length of the peptide increases. To this loss of stability corresponds an increase of the folding of the peptide toward the formation, eventually, of a fully fledged helix with the octapeptide as shown in the ECD spectra of Figure 2. As already shown in Figure 4, the chiroptical signal in the plasmonic reagion disappears with the 3_{10}-helix formation. All this supports the idea that the locking of the proper chiral conformation in the nanoparticle is due to interpeptide interactions. Furthermore, we have independently observed (data not shown) that a nanoparticle passivated with a number of peptides lower than that necessary to fully cover the gold core

surface, *i.e.*, with a monolayer not well packed, does not present any chiroptical signal. Both these observations suggest that the process of loss of chirality involves all peptides in the monolayer in a fashion very similar to what happens to the lipids of the bilayer membrane of a vesicular aggregate when it switches from a liquid crystalline state to a fluid one. Also in that case the process is highly cooperative.

CONCLUSION

In conclusion, our studies established the occurrence of peptide sequence-, main chain length-, and temperature-dependent chiroptical properties in peptide-coated 2 nm diameter gold nanoparticles. These properties were detected for the first time in nanoparticles of such a relatively large diameter with the appearance of moderately strong ECD signals in the 300−650 nm wavelength region, corresponding to the gold nanoparticle's quantized electronic structure. Although the only chiral amino acid present in the peptide sequences is L-Ala, the ECD spectra are almost mirror images like those of enantiomers according to the number of amino acids in the main chain (odd or even) or, more likely, in accordance with the type of amino acid closest to the gold surface (Aib or L-Ala). Such a behavior appears to be strongly influenced by the secondary structure assumed by the peptides when passivating the nanoparticles and vanishes when the sequence is long enough to assume a 3_{10}-helix conformation. We speculate that the odd peptides, adopting a structure with a partial parallel-β-sheet character and the even one possibly taking advantage of a strong H-bond with a thiol, stabilize different chiral arrangements of the staples placed on the surface of the gold nanocluster. Admittedly, we can only offer a number of clues, but the real nature of the source of the observed phenomena remains elusive. Perhaps a molecular dynamics simulation of the peptide monolayer covering the gold core could help in this regard. This was, however, beyond the scope of this paper. In any case the chirality control we observe is a reversible and cooperative process and can be deactivated or reactivated by increasing or decreasing the temperature.

EXPERIMENTAL SECTION

Peptide Synthesis. All peptides were synthesized following synthetic solution protocols and purified *via* flash chromatography. Physical and chemical characterization are reported in the Supporting Information.

Gold Nanoparticle Synthesis. In a typical experiment Trt-*m*pr-Aib-Ala-OMe (245 mg, 0.41 mmol) and $HAuCl_4 \cdot 3H_2O$ (80 mg, 0.20 mmol) were combined in a 6:4 methanol/Milli-Q water solvent mixture (20 mL). The resulting solution was allowed to stand at 0 °C for 1 h under stirring. To this solution was rapidly added a cold $NaBH_4$ (75 mg, 2.0 mmol) solution in Milli-Q water (2 mL), and the resulting mixture was stirred at room temperature for an additional 2 h. The reaction was quenched by addition of 0.1 M HCl (1 mL). The solvent was removed under reduced pressure to dryness, and the dark residue was dissolved in Milli-Q water (4 mL). Subsequently, the so-obtained solution was first filtered through a 45 μm microfilter and afterward purified *via* size-exclusion gel filtration (eluent: Milli-Q water). Finally, the corresponding AuNp**2** was obtained after lyophilization. The gold nanoparticle structural information was obtained as reported in the Supporting Information.

Conflict of Interest: The authors declare no competing financial interest.

Acknowledgment. The authors thank Prof. L. Di Bari for discussion on the ECD spectra and Dr. R. Schiesari for technical support. Financial support by the Univ. of Padova (PRAT C91J11003560001) and MIUR (PRIN 2010 NRREPL) to A.M., by MIUR (FIRB RINAME contract RBAP114AMK_007) to P.S., and ERC (Starting Grant Project MOSAIC 259014) to F.M. is gratefully acknowledged.

Supporting Information Available: Synthesis, purifications, and characterizations of the peptide ligands (**P2**−**8**) and of the related gold nanoparticles (AuNp**2**−**8**). Determination of AuNp**2**−**8** structural information. Figures of (S1) far-UV ECD spectra and FT-IR absorption spectra of **P2**−**8**; (S2) TEM images of AuNp**2**−**8**; (S3) histograms showing the core size distributions of AuNp**2**−**8**; (S4) TGA analysis of AuNp**2**−**8**; (S5) FT-IR absorption spectrum of AuNp**2**; (S6) FT-IR second-order deconvolution of **P2**−**7**; (S7) UV−vis spectra of AuNps**2**−**8**. This material is available free of charge *via* the Internet at http://pubs.acs.org.

REFERENCES AND NOTES

1. Pasquato, L.; Pengo, P.; Scrimin, P. Functional Gold Nanoparticles for Recognition and Catalysis. *J. Mater. Chem.* **2004**, *14*, 3481–3487.
2. Ojea-Jimenez, I.; Puntes, V. Instability of Cationic Gold Nanoparticle Bioconjugates: The Role of Citrate Ions. *J. Am. Chem. Soc.* **2009**, *131*, 13320–13327.
3. Duchesne, L.; Wells, G.; Fernig, D. G.; Harris, S. A.; Levy, R. Supramolecular Domains in Mixed Peptide Self-Assembled Monolayers on Gold Nanoparticles. *ChemBioChem* **2009**, *9*, 2127–2134.
4. Levy, R. Peptide-Capped Gold Nanoparticles: Towards Artificial Proteins. *ChemBioChem* **2006**, *7*, 1141–1145.
5. Pengo, P.; Polizzi, S.; Pasquato, L.; Scrimin, P. Carboxylate-Imidazole Cooperativity in Dipeptide-Functionalized Gold Nanoparticles with Esterase-Like Activity. *J. Am. Chem. Soc.* **2005**, *127*, 1616–1617.
6. Pengo, P.; Baltzer, L.; Pasquato, L.; Scrimin, P. Substrate Modulation of the Activity of an Artificial Nanoesterase Made of Peptide-Functionalized Gold Nanoparticles. *Angew. Chem., Int. Ed.* **2007**, *46*, 400–404.
7. Free, P.; Shaw, C. P.; Levy, R. PEGylation Modulates the Interfacial Kinetics of Proteases on Peptide-Capped Gold Nanoparticles. *Chem. Commun.* **2009**, 5009–5011.
8. Zaramella, D.; Scrimin, P.; Prins, L. J. Self-Assembly of a Catalytic Multivalent Peptide-Nanoparticle Complex. *J. Am. Chem. Soc.* **2012**, *134*, 8396–8399.
9. Guarise, C.; Pasquato, L.; De Filippis, V.; Scrimin, P. Gold Nanoparticles-Based Protease Assay. *Proc. Natl. Acad. Sci. U.S.A.* **2006**, *103*, 3978–3982.
10. Bonomi, R.; Cazzolaro, A.; Sansone, A.; Scrimin, P.; Prins, L. J. Detection of Enzyme Activity through Catalytic Signal Amplification with Functionalized Gold Nanoparticles. *Angew. Chem., Int. Ed.* **2011**, *50*, 2307–2312.
11. Raha, S.; Paunesku, T.; Woloschak, G. Peptide-Mediated Cancer Targeting of Nanoconjugates. *WIREs Nanomed. Nanobiotechnol.* **2011**, *3*, 269–281.
12. Huang, X.; Peng, X.; Wang, Y.; Wang, Y.; Shin, D. M.; El-Sayed, M. A.; Nie, S. A Reexamination of Active and Passive Tumor Targeting by Using Rod-Shaped Gold Nanocrystals and Covalently Conjugated Peptide Ligands. *ACS Nano* **2010**, *4*, 5887–5896.

13. Ghosh, P. S.; Kim, C. K.; Han, G.; Forbes, N. S.; Rotello, V. M. Efficient Gene Delivery Vectors by Tuning the Surface Charge Density of Amino Acid-Functionalized Gold Nanoparticles. *ACS Nano* **2008**, *2*, 2213–2218.
14. Yan, X.; Blacklock, J.; Li, J.; Möhwald, H. One-Pot Synthesis of Polypeptide Gold Nanoconjugates for *in Vitro* Gene Transfection. *ACS Nano* **2012**, *6*, 111–117.
15. Schaaff, T. G.; Knight, G.; Shafigullin, M. N.; Borkman, R. F.; Whetten, R. L. Isolation and Selected Properties of a 10.4 kDa Gold: Glutathione Cluster Compound. *J. Phys. Chem. B* **1998**, *102*, 10643–10646.
16. George, J.; Thomas, G. Surface Plasmon Coupled Circular Dichroism of Au Nanoparticles on Peptide Nanotubes. *J. Am. Chem. Soc.* **2010**, *132*, 2502–2503.
17. Shukla, N.; Bartel, M. A.; Gellman, A. J. Enantioselective Separation on Chiral Au Nanoparticles. *J. Am. Chem. Soc.* **2010**, *132*, 8575–8580.
18. Rezanka, P.; Zaruba, A.; Kral, V. Supramolecular Chirality of Cysteine Modified Silver Nanoparticles. *Colloids Surf., A* **2011**, *374*, 77–83.
19. Häkkinen, H. The Gold-Sulfur Interface at the Nanoscale. *Nat. Chem.* **2012**, *4*, 443–455.
20. Gautier, C.; Bürgi, T. Chiral Gold Nanoparticles. *ChemPhysChem* **2009**, *10*, 483–492.
21. Jadzinsky, P. D.; Calero, G.; Ackerson, C. J.; Bushnell, D. A.; Kornberg, R. D. Structure of a Thiol Monolayer-Protected Gold Nanoparticle at 1.1 Å Resolution. *Science* **2007**, *318*, 430–433.
22. Rio-Echevarria, I.; Tavano, R.; Causin, V.; Papini, E.; Mancin, F.; Moretto, A. Water-Soluble Peptide-Coated Nanoparticles: Control of the Helix Structure and Enhanced Differential Binding to Immune Cells. *J. Am. Chem. Soc.* **2011**, *133*, 8–11.
23. Schade, M.; Moretto, A.; Donaldson, P.; Toniolo, C.; Hamm, P. Vibrational Energy Transport through a Capping Layer of Appropriately Designed Peptide Helices over Gold Nanoparticles. *Nano Lett.* **2010**, *11*, 3057–3061.
24. Longo, E.; Moretto, A.; Formaggio, F.; Toniolo, C. The Critical Main-Chain Length for Helix Formation in Water: Determined in a Peptide Series with Alternating Aib and Ala Residues Exclusively and Detected with ECD Spectroscopy. *Chirality* **2011**, *23*, 756–760.
25. Hostetler, M. J.; Wingate, J. E.; Zhong, C.-J.; Harris, J. E.; Vachet, R. W.; Clark, M. R.; Londono, J. D.; Green, S. J.; Stokes, J. J.; Wignall, G. D.; *et al*. Alkanethiolate Gold Cluster Molecules with Core Diameters from 1.5 to 5.2 nm: Core and Monolayer Properties as a Function of Core Size. *Langmuir* **1998**, *14*, 17–30.
26. Fabris, L.; Antonello, S.; Armelao, L.; Donkers, R. L.; Polo, F.; Toniolo, C.; Maran, F. Gold Nanoclusters Protected by Conformationally Constrained Peptides. *J. Am. Chem. Soc.* **2006**, *128*, 326–336.
27. Barth, A.; Zscherp, C. Q. What Vibrations Tell us About Proteins. *Rev. Biophys.* **2002**, *35*, 369–430.
28. Arrondo, J. L. R.; Muga, A.; Castresana, J.; Goni, F. M. Quantitative Studies of the Structure of Proteins in Solution by Fourier-Transform Infrared-Spectroscopy. *Prog. Biophys. Mol. Biol.* **1993**, *59*, 23–56.
29. Shaw, C. P.; Middleton, D. A.; Volk, M.; Levy, R. Amyloid-Derived Peptide Forms Self-Assembled Monolayers on Gold Nanoparticle with a Curvature-Dependent β-Sheet Structure. *ACS Nano* **2012**, *6*, 1416–1426.
30. Dolamic, I.; Knoppe, S.; Dass, A.; Bürgi, T. First Enantioseparation and Circular Dichroism Spectra of Au_{38} Clusters Protected by Achiral Ligands. *Nat. Commun.* **2012**, *3*, 798–803.
31. Qian, H.; Eckenhoff, W. T.; Zhu, Y.; Pintauer, T.; Jin, R. Total Structure Determination of Thiolate-Protected Au_{38} Nanoparticles. *J. Am. Chem. Soc.* **2010**, *132*, 8280–8281.
32. Knoppe, S.; Dolamic, I.; Dass, A.; Bürgi, T. Separation of Enantiomers and CD Spectra of $Au_{40}(SCH_2CH_2Ph)_{24}$: Spectroscopic Evidence for Intrinsic Chirality. *Angew. Chem., Int. Ed.* **2012**, *51*, 7589–7591.
33. Knoppe, S.; Dolamic, I.; Bürgi, T. Racemization of a Chiral Nanoparticle Evidences the Flexibility of the Gold-Thiolate Interface. *J. Am. Chem. Soc.* **2012**, *134*, 13114–13120.